PAPER

Check for updates

External environment sensitive circularly polarized luminescence properties of a chiral boron difluoride complex†

Masahiro Ikeshita, [ID] *[a] Hongxi He,[a] Maho Kitahara,[b] Yoshitane Imai [ID] *[b] and Takashi Tsuno [ID] *[a]

A chiral Schiff-base boron difluoride complex bearing a diethylamino group was synthesized. Its photophysical properties were investigated and compared with those of its non-substituted analogue. The complex was found to exhibit solvatofluorochromism with bluish–white emission in moderately polar solvents and intense blue emission in nonpolar solvent. Circularly polarized luminescence (CPL) properties were also examined and it was found that the absolute value of the luminescence dissymmetry factor (g_{lum}) increases significantly in the KBr-dispersed pellet state compared to the solution state. Notably, CPL intensity of the complex enhanced approximately three times upon addition of CH_3SO_3H in CH_2Cl_2. Density functional theory (DFT) calculations were conducted to further understand the photophysical properties.

Introductions

Circularly polarized luminescence (CPL)[1–4] which is defined as differential emission of left- *versus* right-circularly polarized light have attracted increasing attentions over the past decade as an important phenomenon with potential applications in 3D optical displays,[5] biological probes,[6] asymmetric synthesis,[7] as well as CPL lasers.[8] Among the various CPL-active materials, small organic molecules (SOMs)[9] have drawn growing interest owing to the potential application for circularly polarized organic light-emitting diodes (CP-OLEDs).[10] Numerous examples of CPL-SOMs with chiral frameworks such as helicenes,[11] cyclophanes[12] and binaphthyls[13] have been developed and several studies have been reported to establish guidelines for designing molecules that exhibit high CPL efficiency.[11d–g,12g,13f] Controlling CPL characteristics of CPL-SOMs is an important subject in the development of advanced information technologies.[14] One of the strategy to achieve CPL control of SOMs is to design molecules that are sensitive to conformational changes in response to the external environment. To date, a variety of SOMs have been developed in which CPL properties can be controlled depending on the external environment, such as solvent,[15] dispersed matrix[16] and pH.[17]

Organoboron complexes have received increasing attention in recent years due to their efficient and tunable luminescent properties.[18] Such characteristics have led to their wide utilization in optical and optoelectronic devices, including organic light-emitting diodes (OLEDs).[19] Boron difluoride complexes, one of the families of organoboron complexes, have been recognized as promising materials for CPL-SOMs due to their ease of preparation and modification.[20] Various CPL-active boron difluoride complexes[21] containing conjugated π-systems including axial chirality,[21a,c,i] helical chirality[21b,d,h] and planar chirality[21e–g] have been reported.

As part of our program aimed at the creation of novel functional materials with CPL-activities, we have developed organic and organometallic complexes bearing chiral Schiff-base ligands.[16e,21j,22] Previously, we reported that boron difluoride complexes with chiral Schiff-base ligands exhibit multi-colour CPL properties in dilute solution and in the drop cast film state.[21j] In the present work, we aimed to develop novel boron difluoride complexes with controllable CPL properties depending on the external environment for further applications. To this purpose, complex **1a** bearing a diethylamino group was newly designed and the photophysical properties of the complex were compared with the non-substituted analogue **1b** (Fig. 1). As a result, it was found that intensity and colour of CPL can be controlled by varying solvent polarity, dispersed matrix and pH of the solution. Theoretical calculations revealed a relationship between their structures and the photophysical properties including CPL-activities. Herein we describe the synthesis, structure and photophysical properties of chiral Schiff-base boron difluoride complexes with a focus on its tunable CPL properties.

[a]Department of Applied Molecular Chemistry, College of Industrial Technology, Nihon University, Narashino, Chiba 275-8575, Japan. E-mail: ikeshita.masahiro@nihon-u.ac.jp; tsuno.takashi@nihon-u.ac.jp

[b]Department of Applied Chemistry, Faculty of Science and Engineering, Kindai University, 3-4-1 Kowakae, Higashi-Osaka, Osaka 577-8502, Japan. E-mail: y-imai@apch.kindai.ac.jp
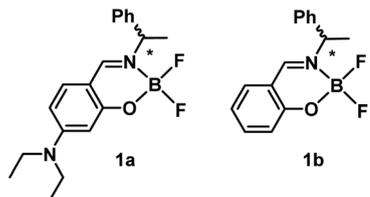
Fig. 1 Structures of the boron difluoride complexes studied in this work.
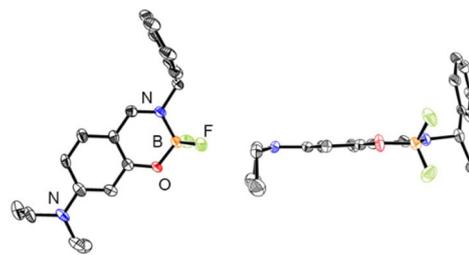

Fig. 2 ORTEP representations of (S)-1a. Left figures: overhead views. Right figures: side views.
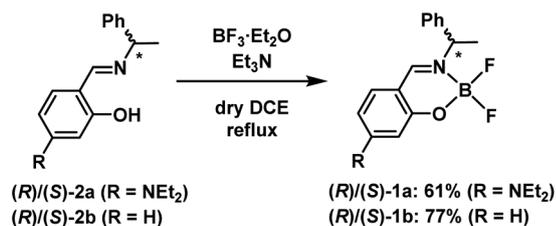
Results and discussion

Synthesis and structures

The chiral boron difluoride complexes (R)-1a and (S)-1a were successfully synthesized by the reaction of $BF_3 \cdot OEt_2$ with optically pure Schiff-base ligands (R)-2a and (S)-2a bearing a diethylamino group in dry 1,2-dichloroethane (DCE) according to the reported procedure (Scheme 1).[20d] The non-substituted analogues (R)-1b and (S)-1b were also prepared as reference compounds from the corresponding optically pure Schiff-base ligands (R)-2b and (S)-2b by the same synthetic methods. The newly synthesized compounds 1a and 2a were successfully characterized by ^1H and ^{13}C nuclear magnetic resonance (NMR) spectroscopy (Fig. S1 and S3, ESI†), infra-red (IR) spectroscopy, high-resolution mass spectrometry (HRMS) and elemental analysis, respectively.

Single crystals of (S)-1a were obtained by recrystallization from a CH_2Cl_2/EtOH solution and the molecular structure was unequivocally established by X-ray diffraction (XRD) analysis at 113 K. The details of the crystal data and the structure refinement are presented in Table S1 (ESI†). ORTEP[23] drawings of (S)-1a are presented in Fig. 2. The boron atoms in (S)-1a adopt a typical tetrahedral geometry to form a six-membered ring which is similar to the previously reported boron difluoride complexes.[20] The packing structure and major interactions in the lattice are shown in Fig. S5 (ESI†). (S)-1a crystallizes in the chiral monoclinic space group $P2_1$. In the lattice, complex (S)-1a was fixed three-dimensional intermolecular H–F bonds.

Photophysical properties

Circular dichroism (CD) and UV-vis absorption spectra of (R)-1a and (S)-1a were recorded in CH_2Cl_2 solution at room temperature (Fig. 3a and b). The spectra of complexes (R)-1b and (S)-1b under the same conditions are also shown for comparison.[20d]
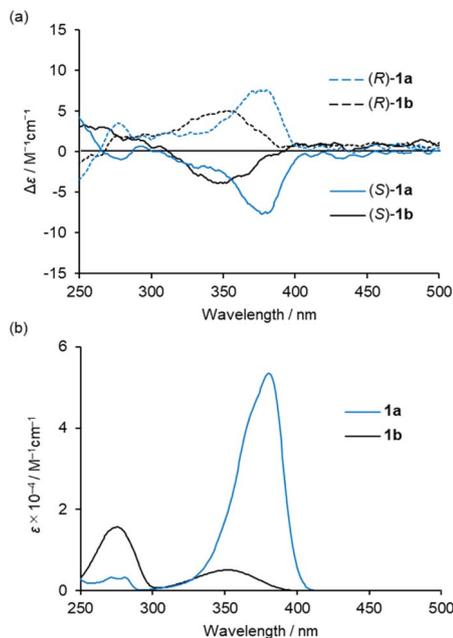

Fig. 3 (a) CD and (b) UV-vis spectra of 2.0×10^{-4} M solutions of 1a and 1b in CH_2Cl_2 at 298 K.

(R)-1a and (S)-1a showed mirror image CD spectra with their maxima matching the maxima of the UV-vis absorption spectra. The low energy band of 1a was increased and bathochromically shifted compared to that of 1b in both CD and UV-vis absorption spectra. This is attributed to the participation of n–π* transition character from the lone pair of the nitrogen atom of the diethylamino group. The $|g_{abs}|$ $(=\Delta\varepsilon/\varepsilon)$ values around the absorption maxima in the low energy region are calculated to be 1.4×10^{-4} (380 nm) for 1a and 1.0×10^{-3} (348 nm) for 1b, respectively. These results indicate that the participation of n–π* increases ε value, resulting in a decrease in the $|g_{abs}|$ value. Further consideration will be discussed in a later section with the results of the theoretical calculations.

Complex 1a exhibited blue to bluish-white luminescence with moderate emission quantum efficiencies (Φ) under UV excitation at room temperature in dilute CH_2Cl_2 solution, in the crystalline and in the KBr-dispersed pellet state, respectively (Fig. 4a). The photophysical data for complexes 1a and 1b are presented in Table 1. The emission spectra in each state are

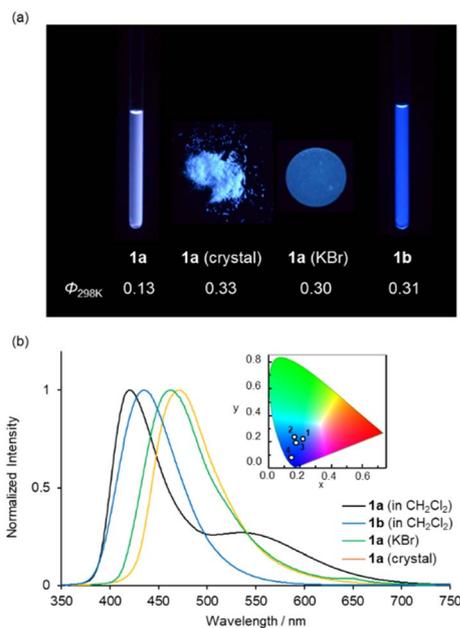Scheme 1 Synthesis of chiral boron difluoride complexes (R)/(S)-1a and 1b.

Fig. 4 (a) Photographs under UV illumination at 365 nm and (b) normalized emission spectra of **1a** and **1b** in CH_2Cl_2 (2.0×10^{-4} M), crystalline and in the KBr-dispersed pellet state at 298 K ($\lambda_{ex} = 350$ nm). The insets in (b) show the CIE colour coordinates of the emissions (1, **1a** in CH_2Cl_2; 2, **1b** in CH_2Cl_2; 3, **1a** (KBr); 4, **1a** (crystal)).

shown in Fig. 4b. In the solution state, complex **1a** exhibited two emission bands around 420 and 540 nm, while **1b** showed only one emission band around 430 nm under the same condition. The emission band around 540 nm in complex **1a** is attributed to the *para*-quinoidal resonance structure in the excited state (Scheme 2).[24] The first emission band in **1a** showed a clear bathochromic shift in the solid state ($\lambda_{max} = 472$ nm for crystal and $\lambda_{max} = 463$ nm for KBr pellet) compared to that of in solution state ($\lambda_{max} = 420$ nm). The CIE colour coordinates plotted on the CIE1931 chromaticity chart[25] (Fig. 4b, inset) indicate that the emission colour of **1a** and **1b** varies between the blue to white region in each state.

While it has been reported that **1b** exhibits identical fluorescent properties in any solvent,[20d] **1a** exhibits
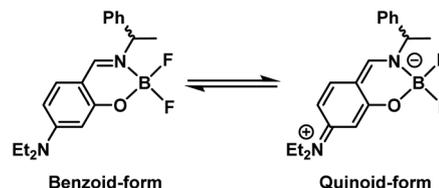
Scheme 2 Plausible equilibrium of the resonance structures of complex **1a** in the excited state.

solvatofluorochromism depending on the polarity of the solvents. Fig. 5a shows photographs of **1a** in various organic solvents under UV irradiation. Bluish-white emissions were observed in moderately polar solvents such as $CHCl_3$, DCE and THF as well as CH_2Cl_2. In nonpolar solvents like toluene, **1a** showed intense blue emission with a high Φ value (0.59) (Fig. 5a). In highly polar solvents (CH_3CN, acetone, DMF and MeOH), **1a** exhibited weak blue emission with a low Φ value (0.01) (Fig. S6 and Table S2, ESI†). The UV-vis absorption spectra of **1a** in various organic solvents are shown in Fig. S7 (ESI†), where identical absorption spectra were observed in all solutions. From these results, we conclude that the polarity of the solvents affects the stability of the resonance structures (benzoid- and quinoid-form) in the excited state which is the key to the dual emission properties of **1a**.

The CPL spectra of the enantiomeric samples **1a** and **1b** in dilute organic solutions show mirror image spectra (Fig. 6 and S8, ESI†), and the emission peak maxima of the CPL signals correspond well to the emission spectra taken under the same measurement conditions (Fig. 4b and 5b). In general, the efficiency of CPL is usually quantified by means of the luminescence dissymmetry factor ($g_{lum} = 2\Delta I/I = 2(I_L - I_R)/(I_L + I_R)$, in which I_L and I_R are the intensity of left- and right-circularly polarized luminescence).[26] The $|g_{lum}|$ values around the maximum emission wavelength in CH_2Cl_2 solution are calculated to be 2.8×10^{-4} (426 nm) for **1a** and 1.0×10^{-3} (433 nm) for **1b**, respectively, which are typical values for small organic and organometallic molecules.[27] The CPL spectra of (*R*)-**1a** and (*S*)-**1a** in toluene, $CHCl_3$, DCE and THF also showed g_{lum} values of the 10^{-4} order (Table 1 and Fig. S8, ESI†). The decrease in the

Table 1 Photophysical data for complexes **1a** and **1b**[a]

Compound	Medium	λ_{abs} [nm]	λ_{max}[b] [nm]	Φ[b,c]	$|g_{lum}|$[d]	CIE (x, y)[b]
1a	CH_2Cl_2	281, 381	420, 539	0.13	2.8×10^{-4} (426 nm)	0.23, 0.21
	$CH_2Cl_2 + CH_3SO_3H$ (10 eq.)	267, 346	423	0.12	9.0×10^{-4} (426 nm)	0.17, 0.09
	Toluene	279, 379	414	0.59	2.3×10^{-4} (423 nm)	0.17, 0.07
	$CHCl_3$	282, 381	417, 534	0.49	2.6×10^{-4} (418 nm)	0.18, 0.12
	DCE	281, 380	421, 546	0.07	2.0×10^{-4} (423 nm)	0.25, 0.22
	THF	279, 375	417, 550	0.04	2.4×10^{-4} (424 nm)	0.22, 0.19
	Crystal	—	472	0.33	—	0.16, 0.23
	KBr pellet	—	463	0.30	2.4×10^{-3} (461 nm)	0.17, 0.20
1b	CH_2Cl_2	354[e]	433[e]	0.32[e]	1.0×10^{-3} (433 nm)	0.15, 0.08

[a] Data were obtained from a 2.0×10^{-4} M solution, crystals or KBr-dispersed pellets at 298 K. [b] $\lambda_{ex} = 350$ nm. [c] Luminescent quantum efficiencies measured using the absolute method with an integrating sphere. [d] The $|g_{lum}|$ values around emission peak maxima are listed. [e] The data for **1b** (reported in ref. 20d) are provided for comparison.
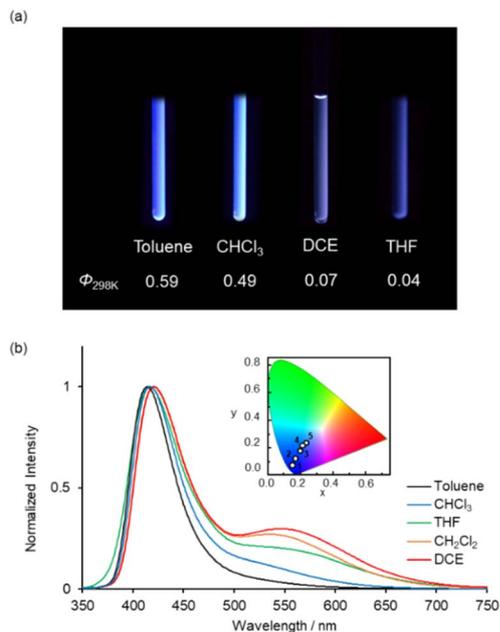

Fig. 5 (a) Photographs under UV illumination at 365 nm and (b) normalized emission spectra of 2.0×10^{-4} M solutions of (S)-**1a** in various organic solvents at 298 K ($\lambda_{ex} = 350$ nm). The insets in (b) show the CIE colour coordinates of the emissions (solvents: 1, toluene; 2, CHCl$_3$; 3, THF; 4, CH$_2$Cl$_2$; 5, DCE).
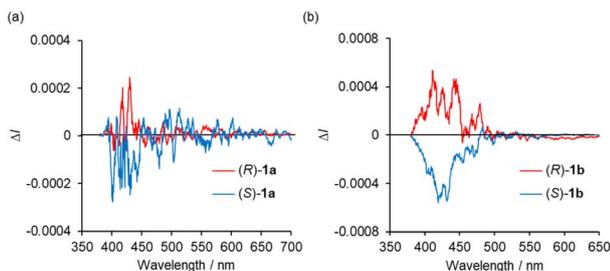

Fig. 6 CPL spectra of (R)-and (S)- (a) **1a** and (b) **1b** in CH$_2$Cl$_2$ (2.0×10^{-4} M) at 298 K ($\lambda_{ex} = 350$ nm).

$|g_{lum}|$ value caused by the introduction of a diethylamino group corresponds to the decrease in the $|g_{abs}|$ value calculated from the CD spectra, which will be also discussed with the results of theoretical calculations described below. The CPL spectra of (R)-**1a** and (S)-**1a** were also recorded in the KBr-dispersed pellet state, showing clear mirror image signals. Their maximum emission $|g_{lum}|$ values are calculated to be 2.4×10^{-3} (461 nm), which is approximately 9 times higher than the value measured in solution (Fig. 7). This improvement of CPL chirality in the KBr-dispersed pellet is considered to be due to the emergence of supramolecular chirality in the aggregated state.

One of the most important photophysical properties of complex **1a** is the acid-induced CPL enhancement, observed in CH$_2$Cl$_2$ upon addition of an excess CH$_3$SO$_3$H. As shown in Fig. 8a, the addition of excess amounts of CH$_3$SO$_3$H (10 equiv.) to a bluish-white emissive solution of complex **1a** in CH$_2$Cl$_2$ typically causes the solution to exhibit blue fluorescence at

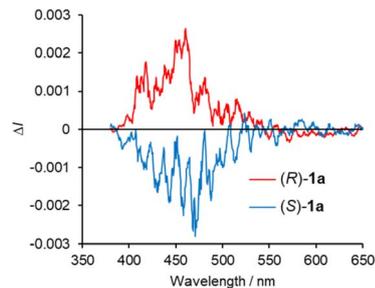**Fig. 7** CPL spectra of (R)-and (S)-**1a** in the KBr-dispersed pellet state at 298 K ($\lambda_{ex} = 350$ nm).

298 K. ^{1}H NMR spectrum of complex **1a** with CH$_3$SO$_3$H in CDCl$_3$ suggests that **1a** is stable under low concentrated acidic solution (Fig. S10†). Fig. 8b and c show changes in the CPL and total emission spectra of 2.0×10^{-4} M solutions of **1a** in CH$_2$Cl$_2$. The addition of CH$_3$SO$_3$H resulted in an increase in CPL intensity around 420 nm (Fig. 8b). In the total emission spectrum, the emission band around 540 nm disappeared (Fig. 8c). The maximum emission $|g_{lum}|$ values in the CPL spectra were calculated to be 9.0×10^{-4} (426 nm), which is approximately 4 times higher than the value measured in the original solution. The UV-vis spectra of **1a** in CH$_2$Cl$_2$ with varying equivalents of CH$_3$SO$_3$H are shown in Fig. S9 (ESI†), where the decrease of n–π* transition band around 380 nm was observed. Hence, the increase in CPL upon acid addition can be attributed to the decrease of n–π* character in the luminescence process.

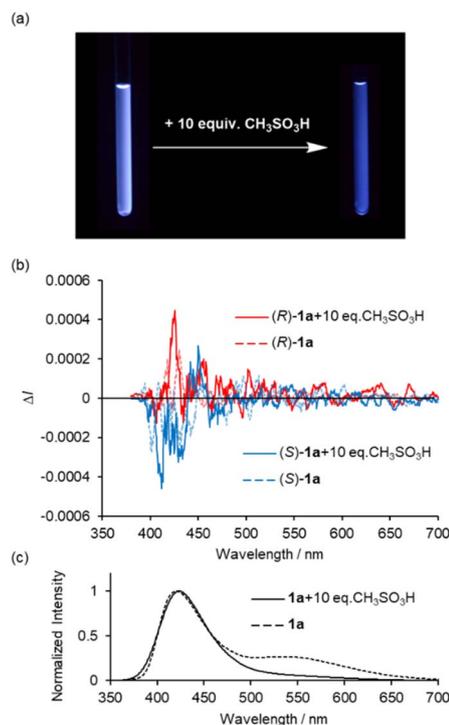**Fig. 8** (a) Photographs under UV illumination at 365 nm, (b) CPL and (c) normalized total emission spectra of (R)- and (S)-**1a** in CH$_2$Cl$_2$ (2.0×10^{-4} M) with and without CH$_3$SO$_3$H at 298 K ($\lambda_{ex} = 350$ nm).

Theoretical calculations

To get more insight into the photophysical properties of the present chiral boron complexes, we performed density functional theory (DFT) and time-dependent (TD) DFT calculations on the B3LYP/6-31+G(d,p) level, using the Gaussian 16 program. The optimized structures and frontier orbitals of (S)-**1a** and (S)-**1b** in the S_0 (ground state) and S_1 (excited state) states were estimated using DFT calculations on the basis of the X-ray structures (Fig. 9). The HOMOs are principally π orbitals of the ligand, including the non-bonding orbital of the diethylamino group of (S)-**1a**, whereas the LUMOs are in the ligand (π^*). The energy levels and electronic configurations of the singlet states of these complexes were estimated from TD-DFT calculations (B3LYP/6-31+G(d,p)) (Tables S3 and S4, ESI†). The major contribution of the electronic configuration of the S_1 states is the HOMO-to-LUMO transition, which implies that the present fluorescence is principally attributable to a mixture of $n-\pi^*$ and $\pi-\pi^*$ transitions of (S)-**1a** and the $\pi-\pi^*$ transition of (S)-**1b**. The S_1-to-S_0 transition energies for S_1 states were calculated to be 2.98 eV (416 nm) for (S)-**1a** and 2.96 eV (419 nm) for (S)-**1b**, which is consistent with the emission peak maxima of the first emission band of the experimental spectra (λ_{max} = 420 nm for (S)-**1a** and λ_{max} = 433 nm for (S)-**1b**).

We considered the variation of chiroptical properties of (S)-**1a** and (S)-**1b** from the viewpoint of transition dipole moments using TD-DFT calculations. The dissymmetry factors g_{abs} for CD and g_{lum} for CPL are calculated with the following equation $g = 4(|\mu_e||\mu_m|\cos\theta_{e,m})/(|\mu_e|^2 + |\mu_m|^2)$, where $|\mu_e|$, $|\mu_m|$ and $\theta_{e,m}$ are the electric transition dipole moments, magnetic transition dipole moments and the angles between the two vectors μ_e and μ_m, respectively.[28] In the case of CPL-SOMs, $|\mu_m|$ is basically much smaller compared with $|\mu_e|$ and can be neglected. Thus, the equation of g can be replaced as follows: $g = 4(|\mu_m|\cos\theta_{e,m}|)/|\mu_e|$, in which the g value is directly proportional to $|\mu_m|$ and inversely proportional to $|\mu_e|$. Fig. 10 shows the electric and magnetic dipole moments calculated for the upward S_0-to-S_1 and the downward S_1-to-S_0 transitions of (S)-**1a** and (S)-**1b** in the optimized geometries. For the upward S_0-to-S_1 transition, g_{abs} values
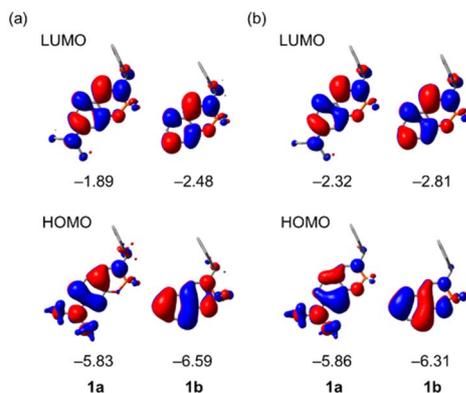

Fig. 9 Molecular orbitals (overhead views) and eigenvalues [eV] for the frontier orbitals of (S)-**1a** and (S)-**1b** estimated from DFT calculations (B3LYP/6-31+G(d,p)) on the basis of the optimized geometries in the (a) S_0 ground and (b) S_1 excited states. Hydrogen atoms are omitted for clarity.
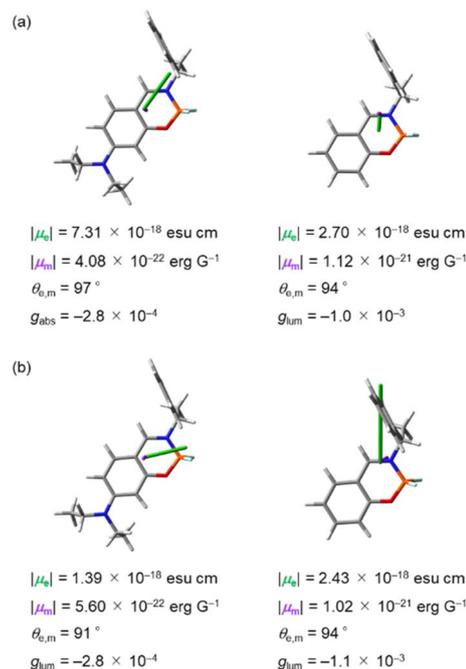

Fig. 10 Electric (μ_e, orange) and magnetic (μ_m, purple) dipole moments of the (a) $S_0 \rightarrow S_1$ transition and (b) $S_1 \rightarrow S_0$ transition for (S)-**1a** (left) and (S)-**1b** (right) calculated at the B3LYP/6-31+G(d,p) level. Calculated values of transition dipole moments ($|\mu_e|$, $|\mu_m|$ and $\theta_{e,m}$) and g_{lum} are given under each structure.

were calculated to be -2.8×10^{-4} for (S)-**1a** and -1.0×10^{-3} for (S)-**1b** (Fig. 10a), which is consistent with the results from experimental CD spectra (-1.4×10^{-4} for (S)-**1a** and -1.0×10^{-3} for (S)-**1b**, Table 1). The scalar values $|\mu_e|$ of (S)-**1a** is more than 2 times higher than that of (S)-**1b**, whereas $|\mu_m|$ was less than half compared to that of (S)-**1b**. Following the equation of the g value, the decrease of the g_{abs} value for (S)-**1a** compared to that of (S)-**1b** is attributed to the changes in the scalar values $|\mu_e|$ and $|\mu_m|$. For the downward S_1-to-S_0 transition, g_{lum} values were calculated to be -2.8×10^{-4} for (S)-**1a** and -1.1×10^{-3} for (S)-**1b** (Fig. 10b) which is consistent with the result from experimental CPL spectra (-2.8×10^{-4} for (S)-**1a** and -1.0×10^{-3} for (S)-**1b**, Table 1). The small g_{lum} for (S)-**1a** can be traced back to the nearly orthogonal electric and magnetic dipole moments: $\theta_{e,m} = 91°$. The angle $\theta_{e,m}$ for the downward transition of (S)-**1b** is $\theta_{e,m} = 94°$. This apparently small change in $\theta_{e,m}$ alone would influence the g_{lum} by a factor of 4 (as $\cos 94°/\cos 91° = 0.07/0.0017$). Given the calculation results, we can be certain that the orientation of dipole moments in the downward S_1-to-S_0 transitions is a key for the decrease in g_{lum} for (S)-**1a** compare to that of (S)-**1b**. The enhancement of the CPL intensity with the addition of CH_3SO_3H was also attributed to the changes in orientation of dipole moments, as the protonation of the diethylamino group reduces the contribution of the $n-\pi^*$ transition character.

Conclusions

In summary, we have demonstrated external environment sensitive circularly polarized luminescence based on Schiff-base

difluoride boron complexes. These chiral compounds exhibited solvatofluorochromism and acid-induced CPL enhancement in the solution state. The CPL intensity was also enhanced in the KBr-dispersed pellet state with a g_{lum} value of 2.4×10^{-3}. DFT and TD-DFT calculations of the structures and electronic configurations of (*S*)-**1a** and (*S*)-**1b** revealed a relationship between molecular structure and photophysical properties. Theoretical consideration of the effect of solvent polarity for solvatofluorochromic behavior observed in **1a** is now in progress.

Author contributions

The project was conceived by Masahiro Ikeshita, who also directed all experiment work, theoretical calculation and wrote the manuscript. Hongxi He performed experimental works except for CPL measurements. Maho Kitahara measured CPL spectra. Yoshitane Imai and Takashi Tsuno gave constructive guidance for this study.

Conflicts of interest

There are no conflicts to declare.

Acknowledgements

Notes and references

1 J. P. Riehl and F. S. Richardson, *Chem. Rev.*, 1986, **86**, 1–16.
2 F. Zinna and L. Di Bari, *Chirality*, 2015, **27**, 1–13.
3 J. P. Riehl and G. Muller, in *Comprehensive Chiroptical Spectroscopy: Instrumentation, Methodologies, and Theoretical Simulations*, John Wiley & Sons, Inc., 2012, vol. 1, pp. 65–90.
4 T. Mori, *Circularly Polarized Luminescence of Isolated Small Organic Molecules*, Springer, 2020.
5 D.-Y. Kim, *J. Korean Phys. Soc.*, 2006, **49**, S505–S508.
6 M. C. Heffern, L. M. Matosziuk and T. J. Meade, *Chem. Rev.*, 2014, **114**, 4496–4539.
7 Y. Inoue, *Chem. Rev.*, 1992, **92**, 741–770.
8 (*a*) J. Jiménez, L. Cerdán, F. Moreno, B. L. Maroto, I. García-Moreno, J. L. Lunkley, G. Muller and S. de la Moya, *J. Phys. Chem. C*, 2017, **121**, 5287–5292; (*b*) D. Qu, M. Archimi, A. Camposeo, D. Pisignao and E. Zussman, *ACS Nano*, 2021, **15**, 8753–8760.

9 (*a*) E. M. Sánchez-Carnerero, A. R. Agarrabeitia, F. Moreno, B. L. Maroto, G. Muller, M. J. Ortiz and S. de La Moya, *Chem.–Eur. J.*, 2015, **21**, 13488–13500; (*b*) N. Chen and B. Yan, *Molecules*, 2018, **23**, 3376.
10 (*a*) J. R. Brandt, F. Salerno and M. J. Fuchter, *Nat. Rev. Chem.*, 2017, **1**, 0045; (*b*) M. Li, S.-H. Li, D. Zhang, M. Cai, L. Duan, M.-K. Fung and C.-F. Chen, *Angew. Chem., Int. Ed.*, 2018, **57**, 2889–2893; (*c*) P. Xue, X. Wang, W. Wang, J. Zhang, Z. Wang, J. Jin, C. Zheng, P. Li, G. Xie and R. Chen, *ACS Appl. Mater. Interfaces*, 2021, **13**, 47826–47834.
11 Helicenes:(*a*) J. E. Field, G. Muller, J. P. Riehl and D. Venkataraman, *J. Am. Chem. Soc.*, 2003, **125**, 11808–11809; (*b*) T. Kaseyama, S. Furumi, X. Zhang and K. Tanaka, *Angew. Chem., Int. Ed.*, 2011, **50**, 3684–3687; (*c*) K. Nakamura, S. Furumi, M. Takeuchi, T. Shibuya and K. Tanaka, *J. Am. Chem. Soc.*, 2014, **136**, 5555–5558; (*d*) H. Tanaka, M. Ikenosako, Y. Kato, M. Fujiki, Y. Inoue and T. Mori, *Commun. Chem.*, 2018, **1**, 38; (*e*) H. Kubo, D. Shimizu, T. Hirose and K. Matsuda, *Org. Lett.*, 2020, **22**, 9276–9281; (*f*) H. Kubo and T. Hirose, *Chem. Lett.*, 2021, **50**, 804–807; (*g*) H. Kubo, T. Hirose, T. Nakashima, T. Kawai, J. Hasegawa and K. Matsuda, *J. Phys. Chem. Lett.*, 2021, **12**, 686–695; (*h*) T. Mori, *Chem. Rev.*, 2021, **121**, 2373–2412.
12 Cyclophanes:(*a*) Y. Morisaki, M. Gon, T. Sasamori, N. Tokitoh and Y. Chujo, *J. Am. Chem. Soc.*, 2014, **136**, 3350–3353; (*b*) M. Gon, Y. Morisaki and Y. Chujo, *J. Mater. Chem. C*, 2015, **3**, 521–529; (*c*) S. P. Morcillo, D. Miguel, L. Alvarez de Cienfuegos, J. Justicia, S. Abbate, E. Castiglioni, C. Bour, M. Ribagorda, D. J. Cardenas, J. M. Paredes, L. Crovetto, D. Choquesillo-Lazarte, A. J. Mota, M. C. Carreno, G. Longhi and J. M. Cuerva, *Chem. Sci.*, 2016, **7**, 5663–5670; (*d*) S. Sato, A. Yoshii, S. Takahashi, S. Furumi, M. Takeuchi and H. Isobe, *Proc. Natl. Acad. Sci. U. S. A.*, 2017, **114**, 13097–13101; (*e*) P. Renie, A. G. Campaña, L. A. de Cienfuegos, V. Blanco, S. Abbate, A. J. Mota, G. Longhi, D. Miguel and J. M. Cuerva, *Chem. Commun.*, 2019, **55**, 10685–10688; (*f*) Y. Morisaki and Y. Chujo, *Bull. Chem. Soc. Jpn.*, 2019, **92**, 265–274; (*g*) N. Miki, R. Inoue and Y. Morisaki, *Bull. Chem. Soc. Jpn.*, 2022, **95**, 110–115.
13 (*a*) T. Kawai, K. Kawamura, H. Tsumatori, M. Ishikawa, M. Naito, M. Fujiki and T. Nakashima, *ChemPhysChem*, 2007, **8**, 1465–1468; (*b*) T. Kimoto, N. Tajima, M. Fujiki and Y. Imai, *Chem.–Asian J.*, 2012, **7**, 2836–2841; (*c*) K. Takaishi, R. Takehara and T. Ema, *Chem. Commun.*, 2018, **54**, 1449–1452; (*d*) K. Takaishi, K. Iwachido, R. Takehana, M. Uchiyama and T. Ema, *J. Am. Chem. Soc.*, 2019, **141**, 6185–6190; (*e*) Y. Nojima, M. Hasegawa, N. Hara, Y. Imai and Y. Mazaki, *Chem. Commun.*, 2019, **55**, 2749–2752; (*f*) Y. Nojima, M. Hasegawa, N. Hara, Y. Imai and Y. Mazaki, *Chem.–Eur. J.*, 2021, **27**, 5923–5929.
14 (*a*) J. Kumar, T. Nakashima and T. Kawai, *J. Phys. Chem. Lett.*, 2015, **6**, 3445–3452; (*b*) J.-L. Ma, Q. Peng and C.-H. Zhao, *Chem.–Eur. J.*, 2019, **25**, 15441–15454; (*c*) F. Song, Z. Zhao, Z. Liu, J. W. Y. Lam and B. Z. Tang, *J. Mater. Chem. C*, 2020, **8**, 3284–3301; (*d*) Y. Gao, C. Ren, X. Lin and T. He,

Front. Chem., 2020, **8**, 458; (*e*) Y. Imai, *Chem. Lett.*, 2021, **50**, 1131–1141.

15 (*a*) A. Statrijio, S. C. J. Meskers and T. M. Swager, *J. Am. Chem. Soc.*, 2006, **128**, 9030–9031; (*b*) Y. Nagata, T. Nishikawa and M. Suginome, *J. Am. Chem. Soc.*, 2014, **136**, 15901–15904; (*c*) Y. Mimura, S. Kitamura, M. Shizuma, M. Kitamatsu, M. Fujiki and Y. Imai, *ChemistrySelect*, 2017, **2**, 7759–7764; (*d*) S. Nakanishi, N. Hara, N. Kuroda, N. Tajima, M. Fujiki and Y. Imai, *Org. Biomol. Chem.*, 2018, **16**, 1093–1100; (*e*) K. Takaishi, K. Iwachido and T. Ema, *J. Am. Chem. Soc.*, 2020, **142**, 1774–1779; (*f*) L. Ji, Y. Liu, Z. Li, G. Ouyang and M. Liu, *Chem. Commun.*, 2021, **57**, 11314–11317.

16 (*a*) T. Kimoto, T. Amako, N. Tajima, R. Kuroda, M. Fujiki and Y. Imai, *Asian J. Org. Chem.*, 2013, **2**, 404–410; (*b*) K. Nakabayashi, T. Amako, N. Tajima, M. Fujiki and Y. Imai, *Chem. Commun.*, 2014, **50**, 13228–13230; (*c*) M. Gon, R. Sawada, Y. Morisaki and Y. Chujo, *Macromolecules*, 2017, **50**, 1790–1802; (*d*) G. Albano, G. Pescitelli and L. Di Bari, *Chem. Rev.*, 2020, **120**, 10145–10243; (*e*) M. Ikeshita, M. Mizugaki, T. Ishikawa, K. Matsudaira, M. Kitahara, Y. Imai and T. Tsuno, *Chem. Commun.*, 2022, **58**, 7503–7506.

17 (*a*) N. Saleh, B. Moore II, M. Srebro, N. Vanthuyne, L. Toupet, J. A. Gareth Williams, C. Roussel, K. K. Deol, G. Muller, J. Autschbach and J. Crassous, *Chem.–Eur. J.*, 2015, **21**, 1673–1681; (*b*) S. Pascal, C. Besnard, F. Zinna, L. D. Rari, B. Le Guennic, D. Jacquemin and J. Lacour, *Org. Biomol. Chem.*, 2016, **14**, 4590–4594; (*c*) H. Sakai, T. Kubota, J. Yuasa, Y. Araki, T. Sakanoue, T. Takenobu, T. Wada, T. Kawai and T. Hasobe, *Org. Biomol. Chem.*, 2016, **14**, 6738–6743; (*d*) T. Otani, A. Tsuyuki, T. Iwachi, S. Someya, K. Tateno, H. Kawai, T. Saito, K. S. Kanyiva and T. Shibata, *Angew. Chem., Int. Ed.*, 2017, **56**, 3906–3910; (*e*) K. Takaishi, M. Yasui and T. Ema, *J. Am. Chem. Soc.*, 2018, **140**, 5334–5338; (*f*) A. H. G. David, R. Casares, J. M. Cuerva, A. G. Campaña and V. Blanco, *J. Am. Chem. Soc.*, 2019, **141**, 18064–18074; (*g*) E. Yen-Pon, F. Buttard, L. Frédéric, P. Thuéry, F. Taran, G. Pieters, P. A. Champagne and D. Audisio, *JACS Au*, 2021, **1**, 807–818.

18 (*a*) F. Jäkle, *Chem. Rev.*, 2010, **110**, 3985–4022; (*b*) Y.-L. Rao and S. Wang, *Inorg. Chem.*, 2011, **50**, 12263–12274; (*c*) G. Wesela-Bauman, P. Ciećwierz, K. Durka, S. Luliński, J. Serwatowski and K. Woźniak, *Inorg. Chem.*, 2013, **52**, 10846–10859; (*d*) D. Frath, J. Massue, G. Ulrich and R. Ziessel, *Angew. Chem., Int. Ed.*, 2014, **53**, 2290–2310; (*e*) M. Gon, K. Tanaka and Y. Chujo, *Bull. Chem. Soc. Jpn.*, 2019, **92**, 7–18.

19 (*a*) H. Yersin, *Highly Efficient OLEDs with Phosphorescent Materials*, Wiley-VCH, Weinheim, 2008; (*b*) L. Xiao, Z. Chen, B. Qu, J. Luo, S. Kong, Q. Gong and J. Kido, *Adv. Mater.*, 2011, **23**, 926–952; (*c*) D. Li, H. Zhang and Y. Wang, *Chem. Soc. Rev.*, 2013, **42**, 8416–8433.

20 (*a*) D. Frath, S. Azizi, G. Ulrich, P. Retailleau and R. Ziessel, *Org. Lett.*, 2011, **13**, 3414–3417; (*b*) Y.-W. Chen, Y.-C. Lin, H.-M. Kuo and C. K. Lai, *J. Mater. Chem. C*, 2017, **5**, 5465–5477; (*c*) M. Urban, K. Durka, P. Jankowski and S. Luliński, *J. Org. Chem.*, 2017, **82**, 8234–8241; (*d*) P. A. A. M. Vaz, J. Rocha, A. M. S. Silva and S. Guieu, *New J. Chem.*, 2018, **42**, 18166–18171.

21 (*a*) F. Zinna, T. Bruhn, C. A. Guido, J. Ahrens, M. Bröring, L. Di Bari and G. Pescitelli, *Chem.–Eur. J.*, 2016, **22**, 16089–16098; (*b*) Y. Gobo, M. Yamamura, T. Nakamura and T. Nabeshima, *Org. Lett.*, 2016, **18**, 2719–2721; (*c*) Z. Jiang, X. Wang, J. Ma and Z. Liu, *Sci. China: Chem.*, 2019, **62**, 355–362; (*d*) C. Maeda, K. Nagahata, T. Shirakawa and T. Ema, *Angew. Chem., Int. Ed.*, 2020, **59**, 7813–7817; (*e*) C.-H. Chen and W.-H. Zheng, *Org. Chem. Front.*, 2021, **8**, 6622–6627; (*f*) K. Li, H. Ji, Z. Yang, W. Duan, Y. Ma, H. Liu, H. Wang and S. Gong, *J. Org. Chem.*, 2021, **86**, 16707–16715; (*g*) W. Duan, H. Ji, Z. Yang, Q. Yao, Y. Huo, X. Ren, J. Zhao and S. Gong, *Dalton Trans.*, 2021, **50**, 12963–12969; (*h*) A. Macé, K. Hamrouni, E. S. Gauthier, M. Jean, N. Vanthuyne, L. Frédéric, G. Pieters, E. Caytan, T. Roisnel, F. Aloui, M. Srebro-Hooper, B. Carboni, F. Berrée and J. Crassous, *Chem.–Eur. J.*, 2021, **27**, 7959–7967; (*i*) L. Cui, H. Shinjo, T. Ichiki, K. Deyama, T. Harada, K. Ishibashi, T. Ehara, K. Miyata, K. Onda, Y. Hisaeda and T. Ono, *Angew. Chem., Int. Ed.*, 2022, **61**, e202204358; (*j*) M. Ikeshita, T. Suzuki, K. Matsudaira, M. Kitahara, Y. Imai and T. Tsuno, *Phys. Chem. Chem. Phys.*, 2022, **24**, 15502–15510.

22 (*a*) M. Ikeshita, S. Furukawa, T. Ishikawa, K. Matsudaira, Y. Imai and T. Tsuno, *ChemistryOpen*, 2022, **11**, e202100277; (*b*) M. Ikeshita, T. Yamamoto, S. Watanabe, M. Kitahara, Y. Imai and T. Tsuno, *Chem. Lett.*, 2022, **51**, 832–835.

23 M. N. Burnett and C. K. Johnson, *ORTEP-III: Oak Ridge Thermal Ellipsoid Plot-Program for Crystal Structure Illustrations, Report ORNL-6895*, Oak Ridge National Laboratory, Oak Ridge, 1996.

24 H. H. T. Al-Sharif, R. Ziessel, P. G. Waddell, C. Dixon and A. Harriman, *J. Phys. Chem. A*, 2020, **124**, 2160–2172.

25 T. Smith and J. Guild, *Trans. Opt. Soc.*, 1931, **33**, 73–134.

26 F. S. Richardson and J. P. Riehl, *Chem. Rev.*, 1977, **77**, 773–792.

27 H. Tanaka, Y. Inoue and T. Mori, *ChemPhotoChem*, 2018, **2**, 386–402.

28 L. Rosenfeld, *Z. Phys.*, 1929, **52**, 161–174.